Ecological Indicators 136 (2022) 108684

Contents lists available at ScienceDirect

Ecological Indicators

journal homepage: www.elsevier.com/locate/ecolind

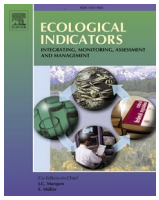

Original Articles

Change in the elevational pattern of vegetation greenup date across the Tianshan Mountains in Central Asia during 2001–2020

Chao Ding [a,*], Wenjiang Huang [b,c], Ming Liu [d,e], Shuang Zhao [f]

[a] Center for Territorial Spatial Planning and Real Estate Studies, Beijing Normal University at Zhuhai 519087, China
[b] State Key Laboratory of Remote Sensing Science, Aerospace Information Research Institute, Chinese Academy of Sciences, Beijing 100094, China
[c] University of Chinese Academy of Sciences, Beijing 100049, China
[d] School of Land Engineering, Chang'an University, Xi'an 710064, China
[e] Xi'an Key Laboratory of Territorial Spatial Information, School of Land Engineering, Chang'an University, Xi'an 710064, China
[f] School of Geology and Geomatics, Tianjin Chengjian University, Tianjin 300384, China

ARTICLE INFO

Keywords:
Land surface phenology
Greenup date
Remote sensing
Elevation gradient
Climate warming
Tianshan Mountains
Central Asia

ABSTRACT

Variations in land surface phenology (LSP) along elevation gradients strongly impact human life and wildlife species distribution across the Tianshan Mountains (TM) in arid and semiarid Central Asia. However, changes in the elevational patterns of LSP in recent decades have not been well understood for the TM. Here, we characterized changes in vegetation greenup date (GUD) and its elevational pattern in the TM and five subregions during 2001–2020, with Moderate Resolution Imaging Spectroradiometer (MODIS) time series of the enhanced vegetation index (EVI). Impacts of land surface temperature (LST) and precipitation on GUD changes were also examined. The results show that GUD changes across the TM were mostly nonsignificant ($P > 0.05$). Approximately 13.4% of the region experienced significant advance in GUD. Furthermore, GUD at low and middle elevations (approximately 1000–2500 m) showed greater proportions of significantly earlier trends. This elevation dependence of GUD changes led to altered elevational patterns of GUD. First, most GUD isolines showed shifts toward higher elevations, and the GUD isolines of day of year (DOY) 110 and 120 located at low and middle elevations exhibited greater mean elevational shifts than those of others for most subregions. Specifically, the mean elevation of the DOY 110 isolines moved from approximately 1325 m to 2126 m in a subregion. Second, increased GUD elevation gradients were observed in several subregions. The spatial pattern of GUD trends may be primarily caused by the increased LST in April, particularly nighttime LST. The results provide information for rangeland management in the context of rangeland degradation across the TM.

1. Introduction

The Tianshan Mountains (TM) across arid and semiarid Central Asia have multiple key ecosystem functions and services. A large area of grasslands in the TM are used as rangelands, and provide abundant food and other resources to humans (Hu, 2004). The TM also serve as important habitats for many wildlife species. However, the ecosystems and human livelihoods in this region are facing multiple environmental threats (de Beurs et al., 2015; Liao et al., 2014b; Lioubimtseva and Henebry, 2009; Yu et al., 2021), such as land degradation (Hu, 2004; Lemenkova, 2014) and biodiversity loss (IPBES, 2018).

Land surface phenology (LSP), a measure of vegetation seasonality over a landscape (de Beurs and Henebry, 2004; Henebry and de Beurs, 2013), has substantial impacts on ecosystem processes and functions (Richardson et al., 2013; Silveira et al., 2021). In high mountainous regions, the spatial patterns of some LSP metrics generally exhibit dependence on elevation due to temperature differences. Both human life and wildlife species activities are related to the elevational patterns of LSP in the TM. Alpine transhumance is the traditional grazing pattern as affected by the differences in LSP across elevations, and overgrazing has caused widespread rangeland degradation in this region (Zhao et al., 2007; Hoppe et al., 2016; Huang et al., 2018). The spatial patterns of LSP metrics and their changes are valuable for guiding the adaptation of transhumance patterns for rangeland restorations (Browning et al., 2019; Matongera et al., 2021). On the other hand, there is distinct elevation dependence of the spatial distribution and seasonal motivation of many wildlife species across the TM (Hu et al., 2004). Previous studies have shown that the timing of vegetation greenup determines the food

* Corresponding author.
E-mail address: dingchao@bnu.edu.cn (C. Ding).

https://doi.org/10.1016/j.ecolind.2022.108684
Received 2 January 2022; Received in revised form 11 February 2022; Accepted 12 February 2022
Available online 18 February 2022

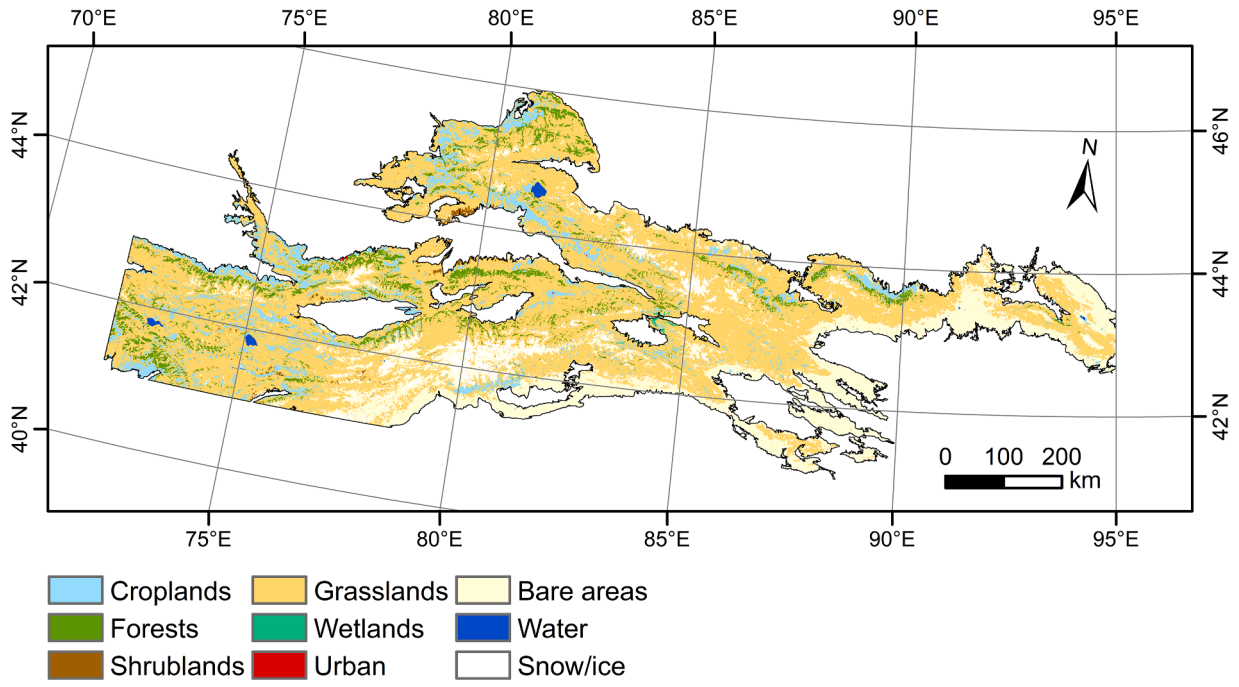

Fig. 1. Land cover map of the year 2001 across the Tianshan Mountains (TM) derived from the ESA CCI product.

abundance of herbivores in spring and therefore affects their spatial distribution and motivation in other regions (Merkle et al., 2016; Oeser et al., 2019). In short, knowledge of variations in LSP, especially the elevational patterns, is valuable for mitigating multiple environmental concerns across the TM.

Previous studies have reported asynchronized changes in vegetation phenology across elevations (e.g., Piao et al., 2011; Thompson and Paull, 2017) and altered elevational gradients of phenology as a result of elevation-dependent temperature changes (e.g., Vitasse et al., 2018; Dai et al., 2021). For example, Vitasse et al. (2018) found a decreased elevation gradient of tree leaf out dates in Europe during the last five decades mainly caused by an increased chilling degree days at higher elevations. An increased elevation gradient of vegetation greenup date (GUD) during 2000–2011 was observed on the Qinghai-Tibetan Plateau (Shen et al., 2014). Misra et al. (2021) reported the differences in spring phenology elevation gradients at higher and lower elevation varied in response to winter and spring temperature changes in the Bavarian Alps, Germany. These studies reflected a spatially heterogeneous nature of changes in spring phenology elevation gradients across the globe.

Multiple studies suggest that the TM experienced a warming climate in recent decades (e.g., Deng et al., 2015; Li et al., 2021b; Xu et al., 2018; Zhang et al., 2021). For example, Deng et al. (2015) reported a stronger increase in daily minimum temperature at low and middle elevations in the Kaidu River Basin in the TM during 1958–2010. Meanwhile, earlier GUDs in the last several decades across the TM have been observed based on satellite remote sensing data (e.g., Dilixiati et al., 2019; Zhang et al., 2019; Li et al., 2021a; Wu et al., 2021). Using the Advanced Very High Resolution Radiometer (AVHRR) NDVI dataset, Li et al. (2021a) revealed a large area of significantly advanced GUD over the TM from 1982 to 2014. Studies using the Moderate Resolution Imaging Spectroradiometer (MODIS) C5 phenological product (2001–2014, Dilixiati et al., 2019) and C6 reflectance product (2000–2019, Wu et al., 2021) also found many earlier GUDs, of which most were non-significant. Meanwhile, these studies also characterized the elevation gradients of GUD across the TM over the entire study periods (Dilixiati et al., 2019; Wu et al., 2021). GUD trends may have led to altered GUD elevational pattern if the trends across elevations were asynchronized in the TM. However, to our knowledge, shifts in the elevational pattern of GUD, which are important for regional ecology and land management, have not been well characterized across the TM.

The objective of this research was to characterize changes in the spatial pattern of GUD along the elevation gradient across the TM for the period of 2001–2020. We used MODIS land surface reflectance data at 500 m spatial resolution to estimate GUD. The following three questions were addressed: (1) Do GUD changes show elevation dependence across the TM? (2) Are there shifts in the spatial pattern of GUD along the elevation gradient? And (3) how do temperature and precipitation affect GUD changes?

2. Materials and methods

2.1. Study area

The study area (72-95°E, 41-46°N) covers the majority of the TM across Central Asia (Fig. 1). To characterize the GUD elevational pattern, we focused on areas containing mountains and parts of the mountain front plains. The study area was eliminated based on elevation and slope (Kapos et al., 2000), with elevation>500 m a.s.l. and slope>1.5°. The elevation and slope were derived from the NASADEM product with a spatial resolution of 30 m (NASA JPL, 2020) obtained from the Google Earth Engine (GEE) platform. We only analyzed areas with continuous mountains. Mountains apart from the continuously mountainous region were excluded. Furthermore, small voids (areas smaller than 1000 km^2) within the continuously mountainous region were filled. Located in an arid and semiarid climate zone, the major vegetation types over the TM are grasslands with multiple subtypes along the elevation gradient (Hu, 2004). Desert vegetation is widespread at lower elevations. Forest belts are generally distributed at middle elevations, particularly on northern slopes of the TM. Above the forest belts, the dominant vegetation types are alpine steppe and alpine meadow.

2.2. Data and preprocessing

2.2.1. MODIS land surface reflectance

The 500 m MOD09A1 C6 land surface reflectance time series data (8-day interval, Vermote, 2015) during 2001–2020 were obtained from

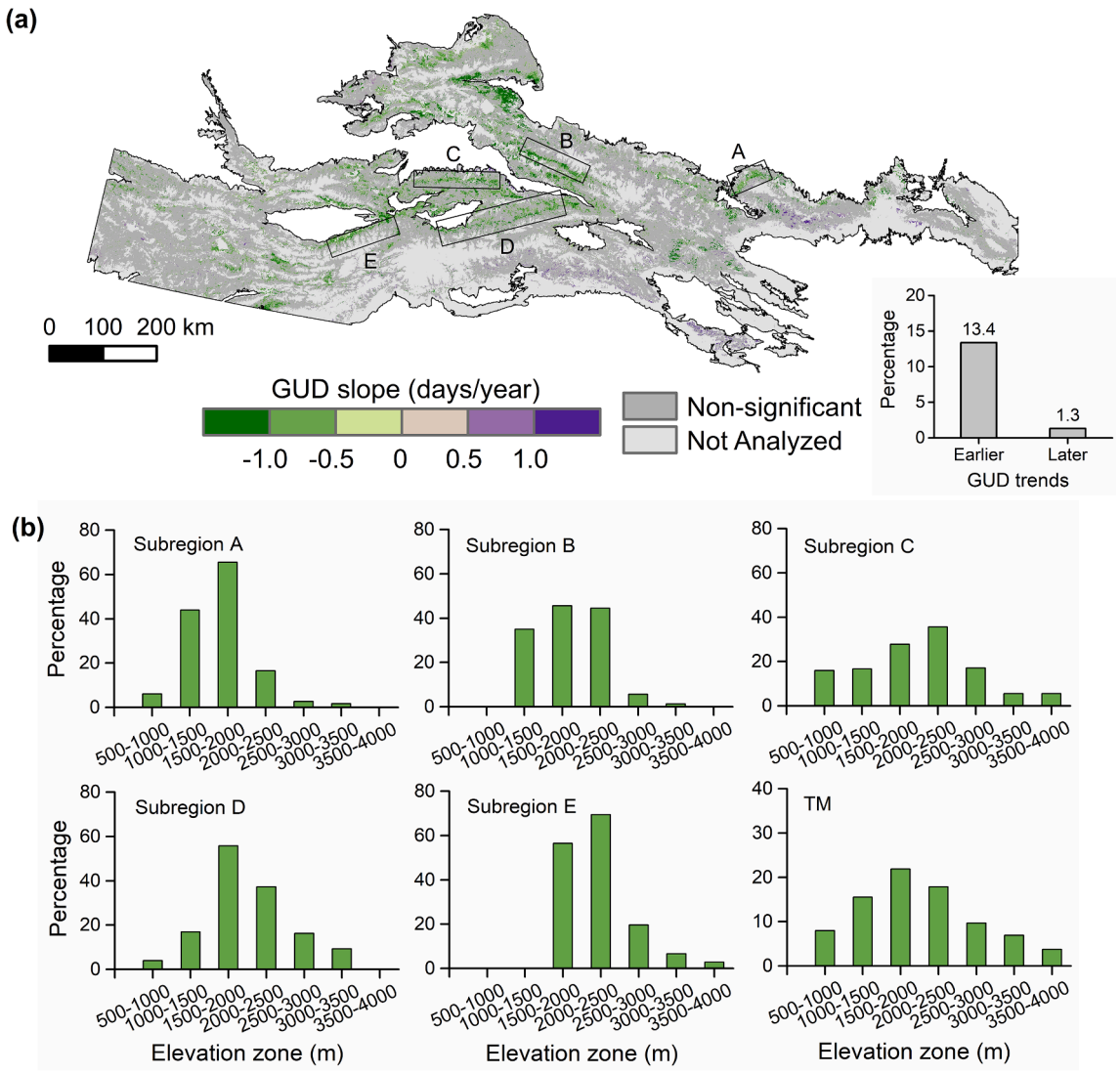

Fig. 2. (a) Spatial distribution of vegetation greenup date (GUD) trends across the TM during 2001–2020, and (b) the proportions of significantly earlier GUD ($p \leq 0.05$) for different elevation zones.

https://ladsweb.modaps.eosdis.nasa.gov/. We calculated the enhanced vegetation index (EVI, Huete et al., 2002) for the retrieval of GUD. The normalized difference snow index (NDSI, Hall and Riggs, 1995) was used to identify observations affected by seasonal snow cover in the EVI time series.

2.2.2. MODIS land surface temperature

We obtained the MOD11A2 C6 8-day average land surface temperature (LST) data with a 1000 m spatial resolution (Wan et al., 2015) during 2001–2020 from https://ladsweb.modaps.eosdis.nasa.gov/. Dilixiati et al. (2019) reported very strong linear correlations between the MOD11A2 LST and the weather station observed air temperature for the TM in Xinjiang, China. GUD was found to have different responses to preseason minimum and maximum temperatures in some regions (e.g., Shen et al., 2016; Hou et al., 2018). Therefore, we used LST in both daytime (LSTD) and nighttime (LSTN) in this research. For each pixel, we removed the low-quality LST estimates in the LSTD and LSTN time series based on the quality control layers. We then filled the gaps in the time series using linear interpolation. The gap filled LSTD and LSTN were resampled to a 500 m spatial resolution using bilinear interpolation. To investigate the effects of spring temperature on GUD changes, we calculated six monthly average LST variables, including LSTD in March (day of year (DOY) 57–88, $LSTD_{MAR}$), LSTN in March ($LSTN_{MAR}$), LSTD in April (DOY 89–120, $LSTD_{APR}$), LSTN in April ($LSTN_{APR}$), LSTD in May (DOY 121–152, $LSTD_{MAY}$), and LSTN in May ($LSTN_{MAY}$). Preseason temperature is a widely used temperature metrics for phenological studies (e.g., Jeong et al., 2011; Shen et al., 2016). Here, we used fixed periods rather than pixel-tuned preseason to allow a spatial comparison of LST trends among pixels (Piao et al., 2011).

2.2.3. ERA5-land monthly precipitation

We obtained the ERA5-land monthly precipitation (Muñoz-Sabater et al., 2021) during 2001–2020 from the Copernicus climate change service (https://cds.climate.copernicus.eu/about-c3s). This reanalysis dataset has a spatial resolution of 0.1°. The ERA5 precipitation data were reported to have good performance in Central Asia (Zandler et al., 2020; Rakhmatova et al., 2021) and China (Jiao et al., 2021). We calculated the total precipitation from January to April (TP_{JA}) for each year, and then resampled the TP_{JA} to a 500 m spatial resolution using bilinear interpolation.

2.2.4. ESA CCI land cover map

We used the ESA CCI land cover map (300 m spatial resolution) for the year 2001 (Santoro et al., 2017) from http://maps.elie.ucl.ac.be/CCI/viewer/. We combined the original 22 land cover types into nine types (Fig. 1), and then resampled the combined map to a 500 m

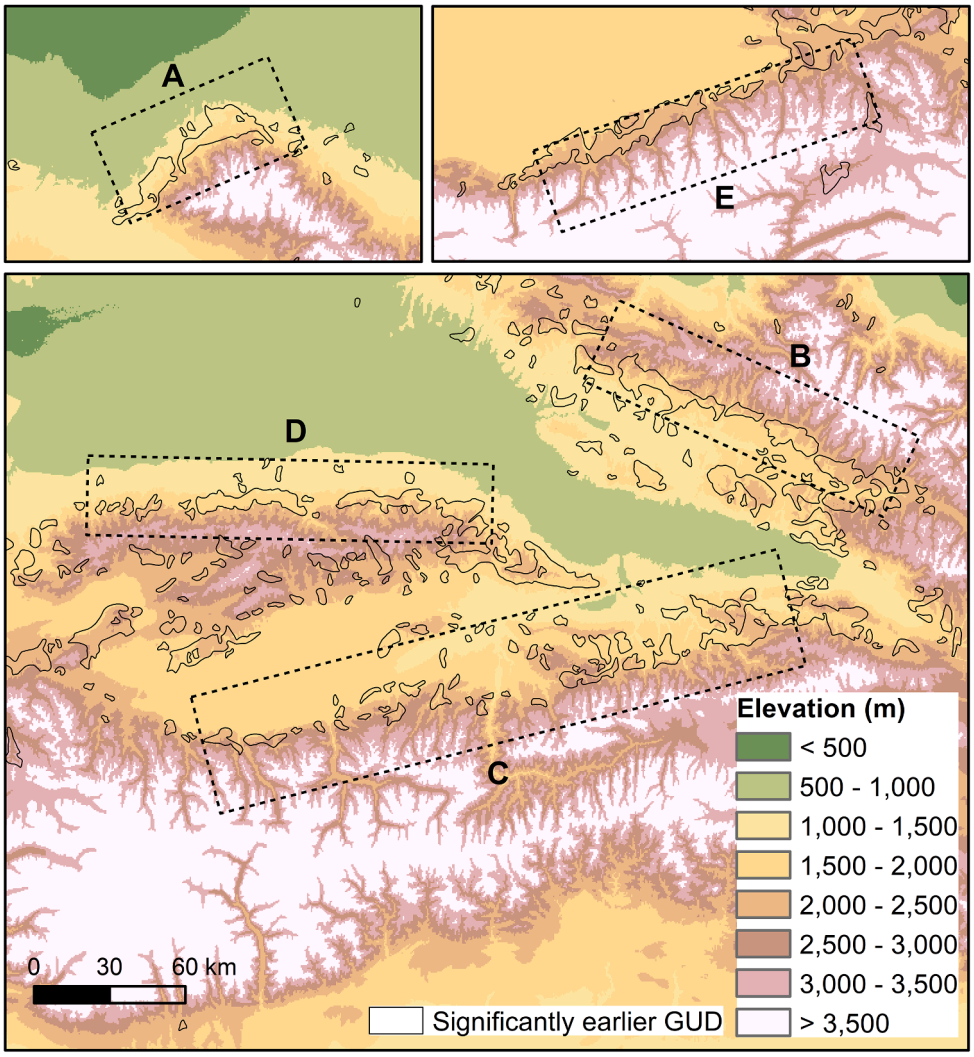

Fig. 3. Overlay of the significantly earlier GUD on the DEM over the five subregions. The polygons of the earlier GUD were converted from the raster layer of GUD trend. Polygons with areas smaller than 5 km^2 were removed, and small voids within the polygons were filled. We smoothed the boundaries of the polygons with the polynomial approximation with exponential kernel algorithm (Bodansky et al., 2002).

spatial resolution. The combined grasslands consist of the original ESA CCI grassland, sparse vegetation, and natural vegetation/cropland mosaic. Forests are the combination of all forest types and the two mosaic types of natural vegetation. GUD change analyses were performed for grasslands, forests, and shrublands.

2.3. Smoothing of the EVI time series and retrieval of GUD

We removed low-quality observations (i.e., clouds, cloud shadows, and snow) and then filled the gaps and smoothed the EVI time series following Ding et al. (2022). Cloud and cloud shadow observations were identified based on the MOD09A1 quality layer. Snow cover observations were identified using NDSI > 0.1 (Gladkova et al., 2012). For each pixel, we filled the snow contaminated observations with the background EVI value, which was determined using the 5% percentile of all clear EVI values within the most recent five years (Gray et al., 2019). We then filled the cloud contaminated observations in the EVI time series with linear interpolation based on cloud-free EVI values. The asymmetric Gaussian function fitting provided in the TIMESAT 3.3 software was selected to smooth the preprocessed EVI time series (Eklundh and Jönsson, 2017; Jönsson and Eklundh, 2002, 2004). The median filter with a spike parameter value of 1.0 was used to detect remaining spikes in the EVI time series. The detected spikes were excluded from the fitting process. For the fitting process, the iteration times of fitting the upper envelope was three and the fitting strength was three. The timing of 30% seasonal EVI amplitude was determined as GUD.

2.4. Statistical analyses

Monotonic change rates of GUD, LST variables, and TP_{JA} for the 2001–2020 period were characterized using the Sen-Theil slope (Sen, 1968; Theil, 1992). The Man-Kendall trend test was utilized to examine the significance of the slope (Mann, 1945). The Spearman rank correlation analysis was used to examine the relationships between interannual variations in GUD and the six LST variables and the TP_{AJ}. We also performed least square linear regression between the time series of GUD and LST variables and then computed the GUD modeled by each of the six LST variables using the corresponding regression function (Liu et al., 2018). The Sen-Theil slopes of observed and modeled GUDs were compared to further explain the impacts of LST on GUD changes.

We compared the elevational patterns of the mean GUD at the start (2001–2005) and end (2016–2020) of the study period. Changes in the GUD elevational patterns were characterized by (1) elevational shifts of GUD isolines and (2) changes in GUD elevation gradients. The isolines were generated based on the spatial moving average GUD (moving window size 9*9 pixels) to achieve smooth isolines. Short isolines

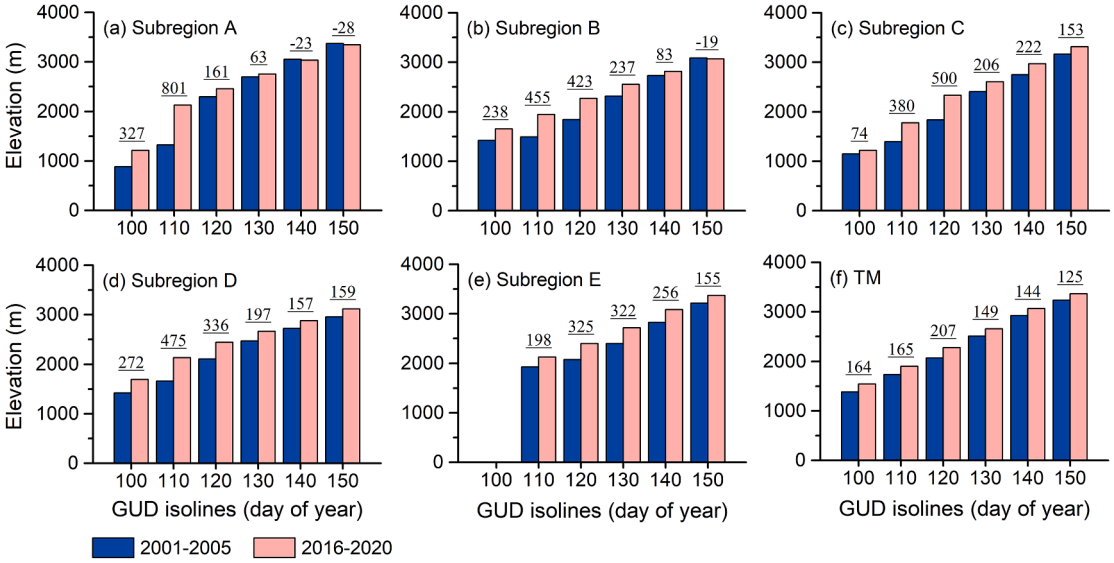

Fig. 4. Mean elevations of the GUD isolines during the start (2001–2005) and end (2016–2020) of the study period. The underlined labels represent the differences in the mean elevations of the GUD isolines between the two periods.

(length < 20 km) were removed from further analyses. In total, six GUD isolines with DOY ranging from 100 to 150 (10-day interval) were selected according to the GUD ranges across the region. Regarding the strongly heterogeneous climate and vegetation composition across the TM, we selected five subregions for detailed analyses. The subregions were delineated according to the following criteria: (1) there were significant trends in GUD, (2) the regions cover either the northern or southern slope of the TM, and (3) the regions were dominated by natural vegetation. The selected subregions are displayed in Fig. 2a. GUD elevation gradients were only analyzed for the five subregions.

3. Results

3.1. Elevation-dependent GUD trends over the 2001–2020 period

Most of the GUD trends across the TM during 2001–2020 were statistically nonsignificant ($p > 0.05$, Fig. 2a). Approximately 13.4% of the region experienced significantly earlier GUD. Significantly later GUD was observed for only 1.3% of the region. We found strong elevation dependence of the GUD changes. Larger proportions of significantly earlier GUD were revealed at low and middle elevations (approximately 1000–2500 m a.s.l.) for the TM (Fig. 2b). This phenomenon also occurred in all subregions despite their different environments. For instance, more than 60% of the pixels experienced significantly earlier GUD across 1500–2000 m a.s.l. in subregion A, while for 2500–3000 m a.s.l. the proportion was smaller than 10%. For all subregions, the largest proportion of significant trend toward earlier GUD was found in elevation zones 1500–2000 m or 2000–2500 m a.s.l.

Fig. 3 displays the overlay of the spatially continuous trends of significantly earlier GUD on the DEM. The earlier GUD showed horizontal zonal distribution patterns in all subregions except for subregion C. Among the subregions, the elevations of the horizontal zones were different. For example, the horizontal zone of subregion D was mainly located between elevations of approximately 1500–2000 m a.s.l. For subregion E, the elevation range was approximately 2000–2500 m a.s.l. The spatial pattern of earlier GUD was fragmented in subregion C but also mainly occurred below an elevation of approximately 2500 m a.s.l. In addition, overlay of the earlier GUD and the land cover map indicates that the earlier GUD trends were mainly located in grasslands and forests around the lower margin of the forest belt in each subregion (Fig. S1).

3.2. Altered GUD elevational pattern

Most GUD isolines showed shifts toward higher elevations between 2001–2005 and 2016–2020 across the TM and the five subregions (Fig. 4). Downward shifts were only observed for the isolines of DOY 140 and 150 in subregion A and the isolines of DOY 150 in subregion B with elevational shifts smaller than 100 m (Fig. 4a and 4b). In 2001–2005, the GUD isolines of DOY 110 and 120 are mainly located at low and middle elevations. And for all regions except for subregion E, the GUD isolines of DOY 110 and 120 exhibited stronger shifts than the others. This phenomenon was more evident in subregion A, with the mean elevation of the DOY 110 isolines shifting from 1325 m to 2126 m a.s.l. The maps of the GUD isolines of DOY 110 and 140 for the five subregions depict the phenomenon clearly (Fig. 5). For example, the DOY 140 isolines in subregion A were very similar, while for the DOY 110 the difference was much more obvious. In addition, horizontal shifts of the DOY 110 isolines were also much greater than those of DOY 140 isolines (Fig. 5). The small horizontal shifts of the DOY 140 isolines with relatively large elevational shifts in subregions C, D, and E were primarily caused by the greater slopes at higher elevations. In short, the shapes of GUD isolines generally showed greater changes at low and middle elevations.

The GUD elevational profiles at the start and end of the study period for the five subregions are displayed in Fig. 6. In subregions A, B and E, we observed increased GUD elevation gradients (≥4.0 days/1000 m) as a result of stronger advances in GUD at low and middle elevations. Although the GUD gradient across the elevation range increased by only 4.0 days/1000 m in subregion A, the shape of the GUD profile obviously altered. The GUD profiles in subregions A and B above 2400 m and 2800 m a.s.l. showed almost no change, respectively. For subregions C and D, although differences in GUD changes across elevations were observed, the differences were not strong enough to alter the GUD gradients. No strong decrease in GUD elevation gradient was found for the five subregions.

3.3. Impacts of LST and precipitation on GUD changes

The Spearman rank correlation coefficients between GUD and the LST variables are provided in Fig. 7. Significant correlations were mostly negative. The proportions of significantly negative correlations of LST in April were the largest among the three months, followed by LST in March. In each month, the spatial patterns of the correlations for daytime and nighttime LST were generally similar, while local spatial

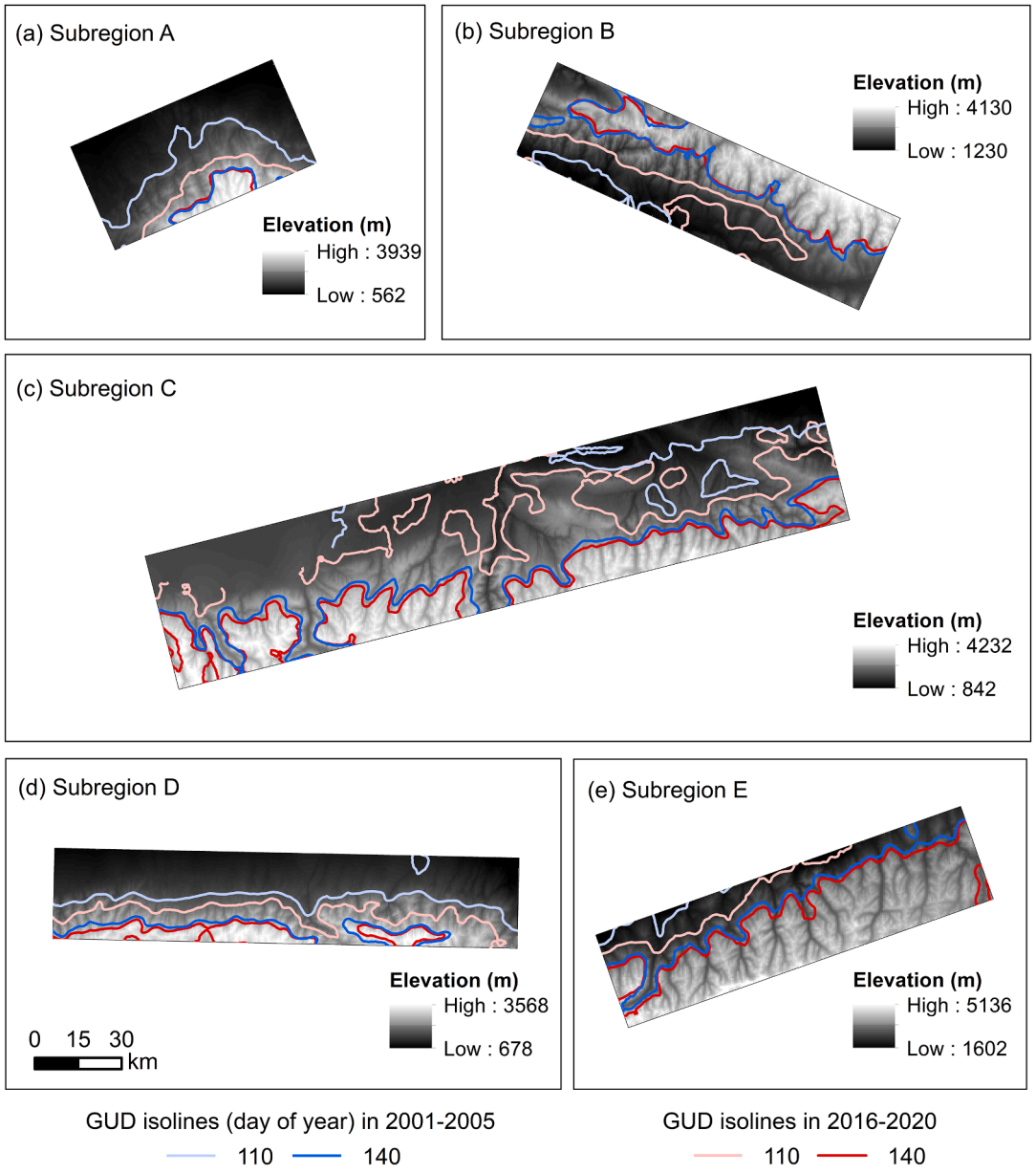

Fig. 5. GUD isolines for days of year (DOY) 110 and 140 at the start and end of the study period over the five subregions.

differences were observed. For the three different months, the spatial patterns were different and showed clear elevation dependence. Significantly negative correlations for March tended to occur at lower elevations, and for May, the significant correlations generally occurred at higher elevations (Fig. 7g). For precipitation, a significantly positive correlation was observed in approximately 14.6% of the region (Fig. 8a).

Fig. 9 presents the spatial distributions of trends in the LST variables for the period 2001–2020. Of the six LST variables, $LSTN_{APR}$ showed the largest proportion of significant increase (38.4%), followed by $LSTD_{APR}$ (12.9%). For other LST variables, rarely significant trends were observed. Trends in TP_{JA} were also mostly nonsignificant (Fig. 8b). The GUD slopes modeled by the six LST variables using linear regression models are provided in Table 1. These modeled GUD changes considered the sensitivities of GUD to LST changes. $LSTN_{APR}$ also showed the strongest explanatory ability for all subregions, particularly for subregions A and B. Furthermore, the spatial pattern of GUD changes modeled by $LSTN_{APR}$ was more consistent with the observed GUD changes than that of $LSTD_{APR}$ (Figs. S2 and S3). These results indicate the important role of $LSTN_{APR}$ in advancing GUD.

4. Discussion

4.1. Changes in GUD and its elevational pattern

We detected changes in MODIS EVI derived GUD across the TM over the period 2001–2020. Approximately 13.4% of the region showed a significantly earlier trend in GUD (Fig. 2b). Earlier GUD trends were also observed in previous studies that used different satellite time series datasets and GUD estimation methods (e.g., Dilixiati et al., 2019; Zhang et al., 2019; Wu et al., 2021). We found the earlier GUD tended to occur at low and middle elevations (approximately 1000–2500 m a.s.l., Fig. 2b and Fig. 3). The elevation-dependent GUD changes have apparently led to altered elevational patterns of GUD. For most subregions, the GUD isolines showed upward shifts with greater shift ranges for the DOY 110 and 120 isolines, which mainly occurred at low and middle elevations (Figs. 4 and 5). Meanwhile, the elevation gradients of GUD increased by $\geq$ 4.0 days/1000 m in three subregions (Fig. 6). A number of studies have reported stronger change rates of spring phenology at higher elevations, for example, in the European Alps (Vitasse et al., 2018) and the

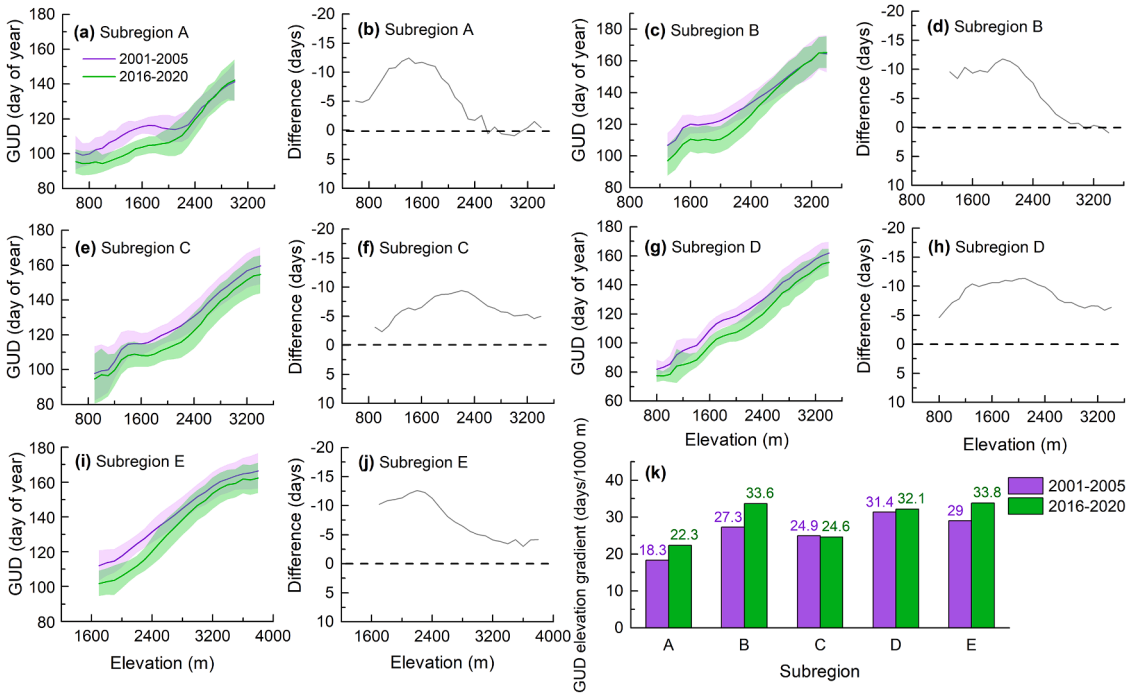

Fig. 6. Elevational profiles of GUD for the start and end of the study period and the differences between them. (a), (b) Subregion A, (c) (d) subregion B, (e) (f) subregion C, (g) (h) subregion D, (i) (j) subregion E. (k) Comparison of GUD elevation gradients between the start and the end of the study period. The error bars represent one standard deviation.

Qinghai-Tibet Plateau (Piao et al., 2011). Stronger advance of spring at higher elevations can result in decreased phenology gradient (e.g., Vitasse et al., 2018; Dai et al., 2021). Using GUD estimated from the $GIMMS_{3g}$ NDVI, Gao et al. (2019) showed that in addition to decreased elevation gradient, increased elevation gradient caused by greater changes at lower elevations was also a widespread GUD change mode over the Northern Hemisphere temperate region. Increase in GUD gradient in the TM was the case of this mode.

The elevation dependence of GUD changes across the TM may be primarily caused by warming in April. First, the negative correlations between GUD and LST variables were elevation dependent. At low and middle elevations, GUD variations were more correlated with LST in March and April (Fig. 7). This is consistent with the concept of preseason temperature. GUD occurs later at higher elevations, and the timing of preseason is also later. Meanwhile, the negative responses of GUD to spring LST were in line with previous studies using air temperature (Kariyeva and van Leeuwen, 2011; Zhang et al., 2019). In terms of daytime and nighttime temperature, we revealed generally similar spatial patterns of the correlations for each month, although there were some local spatial differences (Fig. 7). Using climate data observed from weather stations, Li et al. (2021a) also revealed similar correlations between GUD and minimum and maximum air temperature of alpine grasslands in Xinjiang, China, which covers part of the TM. Second, large areas of significant increase in LST were only observed in April, especially at nighttime. The effects of nighttime and daytime warming in April were also supported by the modeled GUD changes (Table 1, Figs. S2 and S3). Although the modeled GUD changes were smaller than the observed GUD changes, $LSTN_{APR}$ remained the most responsible LST variable for the earlier GUD. The uncertainties may be caused by the following issues: (1) the simple linear regression models cannot explain the possible nonlinear responses of GUD to LST variations, and (2) the MOD11A2 daytime and nighttime LST may not be the optimal LST metrics to model GUD due to the local solar time of the Terra/MODIS sensor observations. On the other hand, TP_{JA} may not be the major factor directly driving earlier GUD across the TM.

4.2. Implications of the altered GUD elevational pattern

The changed GUD elevational pattern has implications for sustainable rangeland management. Rangeland degradation has been one of the major environmental issues restraining sustainable development over the TM for decades (Ludi, 2003; Hu, 2004; Zhumanova et al., 2018). Rest grazing during vegetation greenup periods has been proven to be an effective scheme for restoring rangelands (Li et al., 2017; Fedrigo et al., 2018). In the TM, spring and summer pastures are mainly located at low and middle elevations (Hu, 2004; Liao et al., 2014a). The earlier GUD at low and middle elevations and the changed elevational pattern of GUD provide valuable information for adjusting the periods of rest grazing.

Many significantly earlier GUDs occurred around the lower edge of the forest belt (Fig. S1), a typical forest-grassland ecotone with probably high species richness due to the edge effect. The lower edge of the forest belt may be a hotspot of biodiversity changes for species sensitive to spring vegetation phenology. For example, the major habitats of *Cervus elaphus songaricus*, a typical large herbivore in the TM, are forest and steppe (Hu, 2004). The strong upward shifts of GUD isolines at low and middle elevations may extend the spatial distributions of some herbivore species in spring due to warmer environments and more food (Merkle et al., 2016). In addition, these changing temperature and vegetation phenology may also reduce the habit suitability of some species due to altered species interactions (Plard et al., 2014).

4.3. Limitations

We revealed strong impacts of spring LST on GUD trends across the TM. Previous studies have shown positive correlations between GUD and the end date of snow cover (EDSC) in the European alpines (Xie et al., 2021) and the Qinghai-Tibet Plateau (Wang et al., 2018). For the TM, interannual variations in EDSC during the last two decades were controlled more by spring temperature than by precipitation (Li et al., 2020; Wang et al., 2021). The observed impacts of LST on GUD in this study may also contain the contribution of snowmelt-induced soil moisture variations (Fu et al., 2020). The complex mechanisms of the

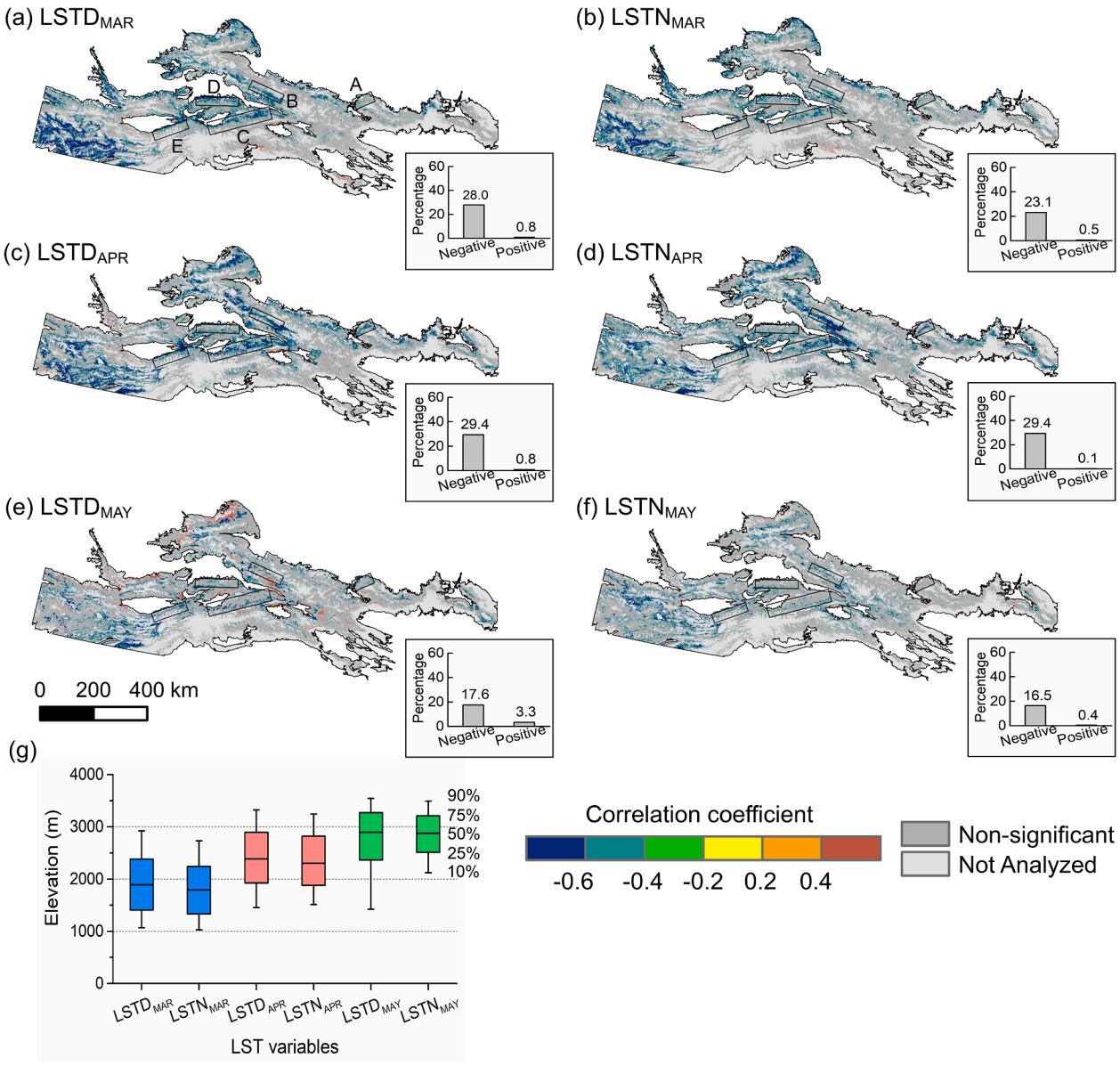

Fig. 7. Spearman correlation coefficients between interannual variations in GUD and land surface temperature (LST) variables (a-f), and box-whisker chart of elevation for pixels showing significantly negative correlations between GUD and LST variables (g).

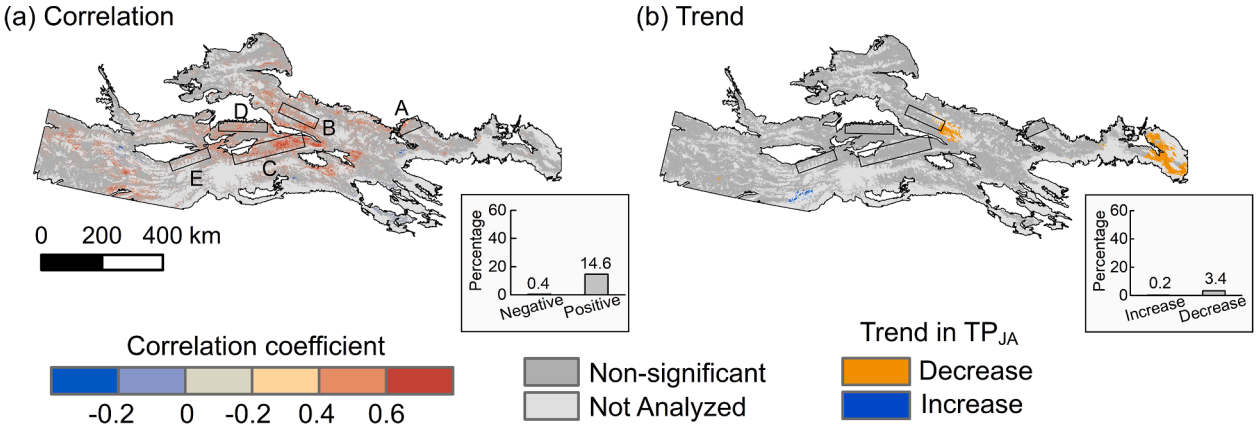

Fig. 8. (a) Spearman correlation coefficients between interannual variations in GUD and total precipitation during January to April (TP_{JA}), and (b) trends in TP_{JA} across the TM during 2001–2020.

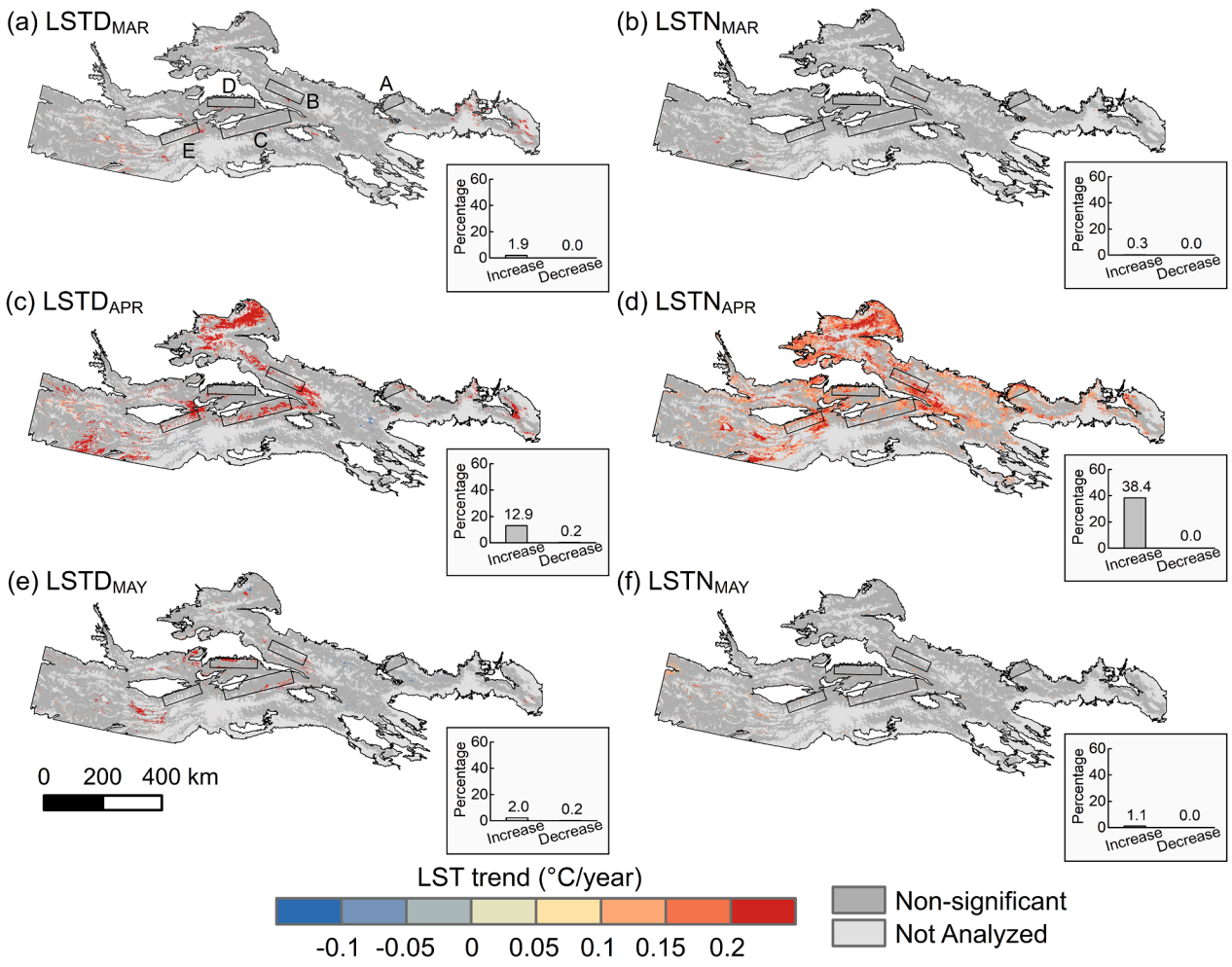

Fig. 9. Trends in the six LST variables during 2001–2020.

Table 1
Average GUD changes (days/year) modeled by the LST variables for different regions. The statistics were computed using only pixels with significant advance in the satellite observed GUD.

Region	Observed	LSTD$_{MAR}$	LSTN$_{MAR}$	LSTD$_{APR}$	LSTN$_{APR}$	LSTD$_{MAY}$	LSTN$_{MAY}$
TM	−0.90	−0.11	−0.09	−0.20	−0.38	−0.08	−0.09
A	−0.89	−0.02	−0.03	−0.26	−0.38	0.01	−0.03
B	−0.93	−0.17	−0.11	−0.32	−0.52	−0.07	−0.15
C	−0.87	−0.13	−0.07	−0.31	−0.30	−0.07	−0.11
D	−0.88	−0.07	−0.05	−0.11	−0.24	−0.09	−0.07
E	−0.85	−0.17	−0.09	−0.25	−0.34	−0.06	−0.11

impacts of temperature, precipitation, and snow melt on GUD in this region require further investigation.

There should be strong mixed pixel effects around the forest-grassland ecotone located at the middle elevations of the TM, as grasslands tend to be located on sunny slopes in such regions and the responses of grassland and forest patches to climate variations within a coarse resolution pixel should be different. Furthermore, aspects can also affect the relationships between GUD and climate factors in the TM within land cover types (Tomaszewska et al., 2020). Although there remain uncertainties, we revealed different contribution between the nighttime and daytime spring LST to the GUD changes. Multiscale analyses integrating coarse, median, and fine spatial resolution satellite data (e.g., de Beurs et al., 2009) are needed to further elucidate LSP variations and the associated drivers for the TM.

5. Conclusions

Changes in GUD across the TM over 2001–2020 were characterized using MODIS time series data. Approximately 13.4% of the region experienced significant trends toward earlier GUD. These earlier GUD trends were generally dependent on elevation, i.e., they tended to occur at low and middle elevations (approximately 1000–2500 m a.s.l.). The elevation-dependent GUD changes induced upward shifts of GUD isolines for most subregions. Meanwhile, increased GUD elevation gradients were observed in three subregions. The spatial pattern of GUD changes may be primarily induced by the warming land surface in April, and particularly induced by nighttime warming. The results provide references for the adjustment of seasonal grazing schemes in the context of combating rangeland degradation. Additionally, the changed elevational pattern of GUD may affect the seasonal distribution of some wildlife species across elevations. Multiscale satellite-based analyses are

expected to provide new insights into the LSP variations over the TM.

CRediT authorship contribution statement

Chao Ding: Conceptualization, Methodology, Formal analysis, Visualization, Writing – original draft, Writing – review & editing. **Wenjiang Huang:** Methodology, Writing – review & editing. **Ming Liu:** Formal analysis, Writing – review & editing. **Shuang Zhao:** Software, Visualization, Writing – review & editing.

Declaration of Competing Interest

The authors declare that they have no known competing financial interests or personal relationships that could have appeared to influence the work reported in this paper.

Acknowledgements

This work was supported by the Central Public-interest Scientific Institution Basal Research Fund (Y2021XK24), the Inner Mongolia Autonomous Region science and technology planning project (2021GG0069), the National Natural Science Foundation of China (42071320), and a grant from Beijing Normal University (310432101). We thank Dr. Jiale Jiang and the anonymous reviewers for their constructive comments on the manuscript.

Appendix A. Supplementary data

Supplementary data to this article can be found online at https://doi.org/10.1016/j.ecolind.2022.108684.

References

Bodansky, E., Gribov, A., Pilouk, M., 2002. Smoothing and compression of lines obtained by raster-to-vector conversion. In: Blostein, D., Kwon, Y.-B. (Eds.), Graphics recognition: algorithms and applications. Springer, Heidelberg, pp. 256–265.

Browning, D.M., Snyder, K.A., Herrick, J.E., 2019. Plant phenology: taking the pulse of rangelands. Rangelands 41 (3), 129–134. https://doi.org/10.1016/j.rala.2019.02.001.

Dai, J., Zhu, M., Mao, W., Liu, R., Wang, H., Alatalo, J.M., Tao, Z., Ge, Q., 2021. Divergent changes of the elevational synchronicity in vegetation spring phenology in North China from 2001 to 2017 in connection with variations in chilling. Int. J. Climatol. 41 (13), 6109–6121. https://doi.org/10.1002/joc.7170.

de Beurs, K.M., Henebry, G.M., Owsley, B.C., Sokolik, I., 2015. Using multiple remote sensing perspectives to identify and attribute land surface dynamics in Central Asia 2001–2013. Remote Sens. Environ. 170, 48–61. https://doi.org/10.1016/j.rse.2015.08.018.

de Beurs, K.M., Henebry, G.M., 2004. Land surface phenology, climatic variation, and institutional change: Analyzing agricultural land cover change in Kazakhstan. Remote Sens. Environ. 89 (4), 497–509. https://doi.org/10.1016/j.rse.2003.11.006.

de Beurs, K.M., Wright, C.K., Henebry, G.M., 2009. Dual scale trend analysis for evaluating climatic and anthropogenic effects on the vegetated land surface in Russia and Kazakhstan. Environ. Res. Lett. 4 (4), 045012. https://doi.org/10.1088/1748-9326/4/4/045012.

Deng, H., Chen, Y., Wang, H., Zhang, S., 2015. Climate change with elevation and its potential impact on water resources in the TM. Central Asia. Glob. Planet. Change 135, 28–37. https://doi.org/10.1016/j.gloplacha.2015.09.015.

Dilixiati, M., Rusuli, Y., Namaiti, H., et al., 2019. The phenological characteristics and climatic response of vegetation in the xinjiang tianshan mountains. China. Climate Change Research 15 (6), 624–632.

Ding, C., Huang, W., Zhao, S., Zhang, B., Li, Y., Huang, F., Meng, Y., 2022. Greenup dates change across a temperate forest-grassland ecotone in northeastern China driven by spring temperature and tree cover. Agric. For. Meteorol. 314, 108780. https://doi.org/10.1016/j.agrformet.2021.108780.

Eklundh, L., Jönsson, P., 2017. Timesat 3.3 Software Manual. Lund and Malmö University, Sweden.

Fedrigo, J.K., Ataide, P.F., Filho, J.A., Oliveira, L.V., Jaurena, M., Laca, E.A., Overbeck, G.E., Nabinger, C., 2018. Temporary grazing exclusion promotes rapid recovery of species richness and productivity in a long-term overgrazed Campos grassland. Restor. Ecol. 26 (4), 677–685. https://doi.org/10.1111/rec.12635.

Fu, Y., Li, X., Zhou, X., Geng, X., Guo, Y., Zhang, Y., 2020. Progress in plant phenology modeling under global climate change. Sci. China Earth Sci. 63 (9), 1237–1247. https://doi.org/10.1007/s11430-019-9622-2.

Gao, M., Piao, S., Chen, A., Yang, H., Liu, Q., Fu, Y.H., Janssens, I.A., 2019. Divergent changes in the elevational gradient of vegetation activities over the last 30 years. Nat. Commun. 10, 1–10. https://doi.org/10.1038/s41467-019-11035-w.

Gladkova, I., Grossberg, M., Bonev, G., Romanov, P., Shahriar, F., 2012. Increasing the accuracy of MODIS/Aqua snow product using quantitative image restoration technique. IEEE Geosci. Remote Sens. Lett. 9 (4), 740–743. https://doi.org/10.1109/LGRS.2011.2180505.

Gray, J., Sulla-Menashe, D., Friedl, M.A., 2019. User Guide to Collection 6 MODIS Land Cover Dynamics (MCD12Q2) Product 6. https://landweb.modaps.eosdis.nasa.gov/QA_WWW/forPage/user_guide/MCD12Q2_Collection6_UserGuide.pdf.

Hall, D.K., Riggs, G.A., 1995. Mapping global snow cover using Moderate Resolution Imaging Spectroradiometer (MODIS) data. Remote Sens. Environ. 54, 127–140.

Henebry, G.M., de Beurs, K.M., 2013. Remote sensing of land surface phenology: A prospectus. In: Schwartz, M.D. (Ed.), Phenology: An Integrative Environmental Science. Springer Netherlands, Dordrecht, pp. 385–411. https://doi.org/10.1007/978-94-007-6925-0_21.

Hoppe, F., Zhusui Kyzy, T., Usupbaev, A., Schickhoff, U., 2016. Rangeland degradation assessment in Kyrgyzstan: vegetation and soils as indicators of grazing pressure in Naryn Oblast. J. Mt. Sci. 13 (9), 1567–1583. https://doi.org/10.1007/s11629-016-3915-5.

Hou, X., Gao, S., Sui, X., Liang, S., Wang, M., 2018. Changes in day and night temperatures and their asymmetric effects on vegetation phenology for the period of 2001–2016 in Northeast China. Can. J. Remote Sens. 44 (6), 629–642. https://doi.org/10.1080/07038992.2019.1578204.

Hu, R.G., 2004. Physical geography of the Tianshan Mountains in China. China Environmental Science Press, Beijing.

Huang, X., Luo, G., Han, Q., 2018. Temporospatial patterns of human appropriation of net primary production in Central Asia grasslands. Ecol. Indic. 91, 555–561. https://doi.org/10.1016/j.ecolind.2018.04.045.

Huete, A., Didan, K., Miura, T., Rodriguez, E.P., Gao, X., Ferreira, L.G., 2002. Overview of the radiometric and biophysical performance of the MODIS vegetation indices. Remote Sens. Environ. 83 (1-2), 195–213. https://doi.org/10.1016/S0034-4257(02)00096-2.

IPBES, 2018. The IPBES regional assessment report on biodiversity and ecosystem services for Europe and Central Asia. In: Rounsevell, M., Fischer, M., Torre-Marin Rando, Mader, A. (Eds.), Secretariat of the Intergovernmental Science-Policy Platform on Biodiversity and Ecosystem. Bonn, Germany.

Jeong, S.J., Ho, C.H., Gim, H.J., Brown, M.E., 2011. Phenology shifts at start vs. end of growing season in temperate vegetation over the Northern Hemisphere for the period 1982–2008. Glob. Chang. Biol. 17, 2385–2399. https://doi.org/10.1111/j.1365-2486.2011.02397.x.

Jiao, D., Xu, N., Yang, F., Xu, K., 2021. Evaluation of spatial-temporal variation performance of ERA5 precipitation data in China. Sci. Rep. 11, 1–13. https://doi.org/10.1038/s41598-021-97432-y.

Jönsson, P., Eklundh, L., 2002. Seasonality extraction by function fitting to time-series of satellite sensor data. IEEE Trans. Geosci. Remote Sens. 40 (8), 1824–1832. https://doi.org/10.1109/TGRS.2002.802519.

Jönsson, P., Eklundh, L., 2004. TIMESAT - A program for analyzing time-series of satellite sensor data. Comput. Geosci. 30 (8), 833–845. https://doi.org/10.1016/j.cageo.2004.05.006.

Kariyeva, J., van Leeuwen, W.J.D., 2011. Environmental drivers of NDVI-based vegetation phenology in Central Asia. Remote Sens. 3, 203–246. https://doi.org/10.3390/rs3020203.

Kapos, V., Rhind, J., Edwards, M., Price, M.F., Ravilious, C., 2000. Developing a map of the world's mountain forests. In: Price, M.F., Butt, N. (Eds.), Forests in sustainable mountain development (IUFRO Research Series 5). CABI Publishing, Wallingford Oxon, pp. 4–9.

Lemenkova, P. 2014. Rural Sustainability and Management of Natural Resources in Tian Shan Region, Central Asia. International Conference Celebrating Pastoral Life. Heritage and Economic Development, CANEPAL European Heritage of Sheep, Farming and Pastoral Life, Sep 2014, Athens, Greece. pp.81-89, 10.6084/m9.figshare.7211927.v2.hal-01963605.

Li, C., Wang, R., Cui, X., Wu, F., Yan, Y., Peng, Q., Qian, Z., Xu, Y., 2021a. Responses of vegetation spring phenology to climatic factors in Xinjiang. China. Ecol. Indic. 124, 107286 https://doi.org/10.1016/j.ecolind.2020.107286.

Li, W., Cao, W., Wang, J., Li, X., Xu, C., Shi, S., 2017. Effects of grazing regime on vegetation structure, productivity, soil quality, carbon and nitrogen storage of alpine meadow on the Qinghai-Tibetan Plateau. Ecol. Eng. 98, 123–133. https://doi.org/10.1016/j.ecoleng.2016.10.026.

Li, Y., Chen, Y., Li, Z., 2020. Climate and topographic controls on snow phenology dynamics in the Tienshan Mountains, Central Asia. Atmos. Res. 236, 104813 https://doi.org/10.1016/j.atmosres.2019.104813.

Li, Y., Chen, Y., Sun, F., Li, Z., 2021b. Recent vegetation browning and its drivers on Tianshan Mountain. Central Asia. Ecol. Indic. 129, 107912 https://doi.org/10.1016/j.ecolind.2021.107912.

Liao, C., Morreale, S.J., Kassam, K.A.S., Sullivan, P.J., Fei, D., 2014a. Following the Green: Coupled pastoral migration and vegetation dynamics in the Altay and TM of Xinjiang. China. Appl. Geogr. 46, 61–70. https://doi.org/10.1016/j.apgeog.2013.10.010.

Liao, C., Sullivan, P.J., Barrett, C.B., Kassam, K.A.S., 2014b. Socioenvironmental threats to pastoral livelihoods: Risk perceptions in the Altay and TM of Xinjiang. China. Risk Anal. 34, 640–655. https://doi.org/10.1111/risa.12146.

Lioubimtseva, E., Henebry, G.M., 2009. Climate and environmental change in arid Central Asia: Impacts, vulnerability, and adaptations. J. Arid Environ. 73, 963–977. https://doi.org/10.1016/j.jaridenv.2009.04.022.

Liu, Y., Chen, Q., Ge, Q., Dai, J., Qin, Y., Dai, L., Zou, X., Chen, J., 2018. Modelling the impacts of climate change and crop management on phenological trends of spring and winter wheat in China. Agric. For. Meteorol. 248, 518–526. https://doi.org/10.1016/j.agrformet.2017.09.008.

Ludi, E., 2003. Sustainable pasture management in Kyrgyzstan and Tajikistan: Development needs and recommendations. Mt. Res. Dev. 23, 119–123. https://doi.org/10.1659/0276-4741(2003)023[0119:SPMIKA]2.0.CO;2.
Mann, H.B., 1945. Nonparametric Tests Against Trend. Econometrica 13, 245–259. https://doi.org/10.2307/1907187.
Matongera, T.N., Mutanga, O., Sibanda, M., Odindi, J., 2021. Estimating and monitoring land surface phenology in rangelands: A review of progress and challenges. Remote Sens. 13, 2060. https://doi.org/10.3390/rs13112060.
Merkle, J.A., Monteith, K.L., Aikens, E.O., Hayes, M.M., Hersey, K.R., Middleton, A.D., Oates, B.A., Sawyer, H., Scurlock, B.M., Kauffman, M.J., 2016. Large herbivores surf waves of green-up during spring. Proc. R. Soc. B Biol. Sci. 283, 1–8. https://doi.org/10.1098/rspb.2016.0456.
Misra, G., Asam, S., Menzel, A., 2021. Ground and satellite phenology in alpine forests are becoming more heterogeneous across higher elevations with warming. Agric. For. Meteorol. 303, 108383 https://doi.org/10.1016/j.agrformet.2021.108383.
Muñoz-Sabater, J., Dutra, E., Agustí-Panareda, A., Albergel, C., Arduini, G., Balsamo, G., Boussetta, S., Choulga, M., Harrigan, S., Hersbach, H., Martens, B., Miralles, D.G., Piles, M., Rodríguez-Fernández, N.J., Zsoter, E., Buontempo, C., Thépaut, J.-N., 2021. ERA5-Land: a state-of-the-art global reanalysis dataset for land applications. Earth Syst. Sci. Data 13, 4349–4383. https://doi.org/10.5194/essd-13-4349-2021.
NASA JPL, 2020. NASADEM Merged DEM Global 1 arc second V001. NASA EOSDIS Land Processes DAAC. https://doi.org/10.5067/MEaSUREs/NASADEM/NASADEM_HGT.001.
Oeser, J., Heurich, M., Senf, C., Pflugmacher, D., Belotti, E., Kuemmerle, T., 2019. Habitat metrics based on multi-temporal Landsat imagery for mapping large mammal habitat. Remote Sens. Ecol. Conserv. 1–18 https://doi.org/10.1002/rse2.122.
Piao, S., Cui, M., Chen, A., Wang, X., Ciais, P., Liu, J., Tang, Y., 2011. Altitude and temperature dependence of change in the spring vegetation green-up date from 1982 to 2006 in the Qinghai-Xizang Plateau. Agric. For. Meteorol. 151, 1599–1608. https://doi.org/10.1016/j.agrformet.2011.06.016.
Plard, F., Gaillard, J.M., Coulson, T., Hewison, A.J.M., Delorme, D., Warnant, C., Bonenfant, C., 2014. Mismatch Between Birth Date and Vegetation Phenology Slows the Demography of Roe Deer. PLoS Biol. 12, 1–8. https://doi.org/10.1371/journal.pbio.1001828.
Rakhmatova, N., Arushanov, M., Shardakova, L., Nishonov, B., Taryannikova, R., Rakhmatova, V., Belikov, D.A., 2021. Evaluation of the perspective of era-interim and era5 reanalyses for calculation of drought indicators for Uzbekistan. Atmosphere. 12 https://doi.org/10.3390/atmos12050527.
Richardson, A.D., Keenan, T.F., Migliavacca, M., Ryu, Y., Sonnentag, O., Toomey, M., 2013. Climate change, phenology, and phenological control of vegetation feedbacks to the climate system. Agric. For. Meteorol. 169, 156–173. https://doi.org/10.1016/j.agrformet.2012.09.012.
Santoro, M.; Kirches, G.; Wevers, J.; Boettcher, M.; Brockmann, C.; Lamarche, C.; Defourny, P., 2017. Land Cover CCI: Product User Guide Version 2.0. http://maps.elie.ucl.ac.be/CCI/viewer/download/ESACCILC-Ph2-PUGv2_2.0.pdf.
Sen, P.K., 1968. Estimates of the Regression Coefficient Based on Kendall's Tau. J. Am. Stat. Assoc. 63, 1379–1389. https://doi.org/10.1080/01621459.1968.10480934.
Shen, M., Piao, S., Chen, X., An, S., 2016. Strong impacts of daily minimum temperature on the green-up date and summer greenness of the Tibetan Plateau. Glob. Chang. Biol. 22, 3057–3066. https://doi.org/10.1111/gcb.13301.
Shen, M., Zhang, G., Cong, N., Wang, S., Kong, W., Piao, S., 2014. Increasing altitudinal gradient of spring vegetation phenology during the last decade on the Qinghai-Tibetan Plateau. Agric. For. Meteorol. 189–190, 71–80. https://doi.org/10.1016/j.agrformet.2014.01.003.
Silveira, E.M.O., Radeloff, V.C., Martinuzzi, S., Martínez Pastur, G.J., Rivera, L.O., Politi, N., Lizarraga, L., Farwell, L.S., Elsen, P.R., Pidgeon, A.M., 2021. Spatio-temporal remotely sensed indices identify hotspots of biodiversity conservation concern. Remote Sens. Environ. 258, 112368 https://doi.org/10.1016/j.rse.2021.112368.
Theil H. 1992. A Rank-Invariant Method of Linear and Polynomial Regression Analysis. In: Raj B., Koerts J. (eds) Henri Theil's Contributions to Economics and Econometrics. Advanced Studies in Theoretical and Applied Econometrics, vol 23. Springer, Dordrecht. 10.1007/978-94-011-2546-8_20.
Thompson, J.A., Paull, D.J., 2017. Assessing spatial and temporal patterns in land surface phenology for the Australian Alps (2000–2014). Remote Sens. Environ. 199, 1–13. https://doi.org/10.1016/j.rse.2017.06.032.
Tomaszewska, M.A., Nguyen, L.H., Henebry, G.M., 2020. Land surface phenology in the highland pastures of montane Central Asia: Interactions with snow cover seasonality and terrain characteristics. Remote Sens. Environ. 240, 111675 https://doi.org/10.1016/j.rse.2020.111675.
Vermote, E., 2015. MOD09A1 MODIS/Terra Surface Reflectance 8-Day L3 Global 500m SIN Grid V006. NASA EOSDIS Land Processes DAAC. https://doi.org/10.5067/MODIS/MOD09A1.006.
Vitasse, Y., Signarbieux, C., Fu, Y.H., 2018. Global warming leads to more uniform spring phenology across elevations. Proc. Natl. Acad. Sci. U. S. A. 115, 1004–1008. https://doi.org/10.1073/pnas.1717342115.
Wan, Z., Hook, S., Hulley, G., 2015. MOD11A2 MODIS/Terra Land Surface Temperature/Emissivity 8-Day L3 Global 1km SIN Grid V006. NASA EOSDIS Land Processes DAAC. https://doi.org/10.5067/MODIS/MOD11A2.006.
Wang, H., Zhang, X., Xiao, P., Zhang, K., Wu, S., 2021. Elevation-dependent response of snow phenology to climate change from a remote sensing perspective: A case survey in the central Tianshan mountains from 2000 to 2019. Int. J. Climatol. 1–17 https://doi.org/10.1002/joc.7330.
Wang, X., Wu, C., Peng, D., Gonsamo, A., Liu, Z., 2018. Snow cover phenology affects alpine vegetation growth dynamics on the Tibetan Plateau: Satellite observed evidence, impacts of different biomes, and climate drivers. Agric. For. Meteorol. 256–257, 61–74. https://doi.org/10.1016/j.agrformet.2018.03.004.
Wu, L., Ma, X., Dou, X., Zhu, J., Zhao, C., 2021. Impacts of climate change on vegetation phenology and net primary productivity in arid Central Asia. Sci. Total Environ. 796, 149055 https://doi.org/10.1016/j.scitotenv.2021.149055.
Xie, J., Hüsler, F., de Jong, R., Chimani, B., Asam, S., Sun, Y., Schaepman, M.E., Kneubühler, M., 2021. Spring Temperature and Snow Cover Climatology Drive the Advanced Springtime Phenology (1991–2014) in the European Alps. J. Geophys. Res. Biogeosciences 126. https://doi.org/10.1029/2020JG006150.
Xu, M., Kang, S., Wu, H., Yuan, X., 2018. Detection of spatio-temporal variability of air temperature and precipitation based on long-term meteorological station observations over TM, Central Asia. Atmos. Res. 203, 141–163. https://doi.org/10.1016/j.atmosres.2017.12.007.
Yu, Y., Chen, X., Malik, I., Wistuba, M., Cao, Y., Hou, D., Ta, Z., He, J., Zhang, L., Yu, R., Zhang, H., Sun, L., 2021. Spatiotemporal changes in water, land use, and ecosystem services in Central Asia considering climate changes and human activities. J. Arid Land 13, 881–890. https://doi.org/10.1007/s40333-021-0084-3.
Zandler, H., Senftl, T., Vanselow, K.A., 2020. Reanalysis datasets outperform other gridded climate products in vegetation change analysis in peripheral conservation areas of Central Asia. Sci. Rep. 10, 1–16. https://doi.org/10.1038/s41598-020-79480-y.
Zhang, R., Guo, J., Liang, T., Feng, Q., 2019. Grassland vegetation phenological variations and responses to climate change in the Xinjiang region. China. Quat. Int. 513, 56–65. https://doi.org/10.1016/j.quaint.2019.03.010.
Zhang, Y., An, C., Liu, L., Zhang, Y.Z., Lu, C., Zhang, W., 2021. High Mountains Becoming Wetter While Deserts Getting Drier in Xinjiang, China since the 1980s. Land. https://doi.org/10.3390/land10111131.
Zhao, W.Y., Li, J.L., Qi, J.G., 2007. Changes in vegetation diversity and structure in response to heavy grazing pressure in the northern TM. China. J. Arid Environ. 68, 465–479. https://doi.org/10.1016/j.jaridenv.2006.06.007.
Zhumanova, M., Mönnig, C., Hergarten, C., Darr, D., Wrage-Mönnig, N., 2018. Assessment of vegetation degradation in mountainous pastures of the Western Tien-Shan, Kyrgyzstan, using eMODIS NDVI. Ecol. Indic. 95, 527–543. https://doi.org/10.1016/j.ecolind.2018.07.060.